Toward Intelligent Adaptive Airborne GPR, Implementation and Data Acquisition

Saeed Haghniaz Jahromi∗†
Worcester, MA, USA
shaghniazjahromi@wpi.edu

Vincent Filardi∗§
Worcester, MA, USA
vfilardi@wpi.edu

Seyed (Reza) Zekavat∗ † §
Worcester, MA, USA
rezaz@wpi.edu

Zhonghai Wang
Alex and Alice Inc.
Chief Technology Office
Boyds, MD, USA
wzhongha@mtu.edu

Joshua Thurber∗§
Worcester, MA, USA
jethurber@wpi.edu

Dylan Hoffman∗§
Worcester, MA, USA
djhoffman@wpi.edu

Charlotte Larson∗§
Worcester, MA, USA
clarson2@wpi.edu

Douglas Petkie∗†
Worcester, MA, USA
dtpetkie@wpi.edu

***Abstract*—This paper is the first attempt toward the realization of intelligent soil subsurface moisture characterization via a pulse-modulated Stepped Frequency Continuous Wave (SFCW) Ground Penetrating Radar (GPR). The GPR design is standalone, autonomous, and drone-rated (compact and light-weight), facilitating the development of an airborne GPR for megafarm moisture assessment. The design also enables the implementation of diverse waveforms for the transmitted signal. Thus, the waveform can adaptively be adjusted to optimally extract the soil subsurface features from the received signal. Based on a measurement campaign conducted in the summer of 2024, the paper assesses the performance of moisture estimation using multiple Machine Learning models applied to the received signal power features across all frequency components of the SFCW waveform. The results confirm the potential of the designed radar for intelligent soil moisture estimation.**

***Index Terms*—Ground Penetrating Radar, Soil Moisture, Pulse-Modulated Stepped Frequency Continuous Wave, Intelligent, Adaptive, Machine Learning**

I. Introduction

Climate change has significantly affected groundwater resources. For instance, in the United States, groundwater resources in many states, including Nebraska, Iowa, and Kansas, are shrinking, and megafarms are among the primary consumers of underground water resources. On the other hand, overwatering washes away critical soil minerals. Therefore, water usage in megafarms should be optimized to avoid waste and maintain soil minerals. Farmers in megafarms apply the same amount of water to the soil. However, the texture and, consequently, the hydraulic water capacity of the soil varies across the vast lands of megafarms [1]. Therefore, it is critical to assess soil texture within megafarms and understand which parts can retain moisture longer. Moisture probe reading is a traditional method to assess soil moisture content. However, the implementation of moisture probes in megafarms is expensive in terms of both equipment and the required manpower. Additionally, logistically, it is challenging to implement moisture probes because the equipment installed in the ground can hinder the processes of planting and harvesting.

Ground Penetrating Radar (GPR) can detect subsurface features by analyzing the reflected signals from the ground. Traditionally, scientists have conducted common mid-point and common off-set scans for the extraction of subsurface features, which were complex and time-consuming processes that required expert opinion. Recently, intelligent GPR has been introduced that maps the received signals to subsurface moisture features through Machine Learning methods [2][3][4][5][6][7]. There are a large number of off-the-shelf GPRs capable of extracting soil subsurface features. For example, AKELA has introduced a Stepped Frequency Continuous Wave (SFCW) radar. The operator can select a set of frequency components within the 0.4-2GHz range, with 40MHz step frequency [2]. AKELA radar has a fixed built-in signal processing technique for transmitted and received signals, which prevents operators from implementing different signal reception methods for any intelligent feature engineering. It integrates the time domain data associated with each frequency component within 0.4 - 2GHz and only returns a set of complex numbers as the received signal associated with the adopted frequency components. Furthermore, the radar is only capable of using SFCW waveform. In addition, AKELA currently holds a commercial license, but because the company is not operational, it is impossible to customize its embedded code to make it compatible with different measurements. As a result, we are unable to retrieve the original time domain data. This prevents us from extracting range bin information and developing other signal processing techniques that could provide a broader range of information and enhance the performance of this radar for soil subsurface characterization.

Moreover, the transmitted signal by GPR interacts with the soil subsurface channel to create the received signal. Thus, the transmitted signal should be properly, optimally,

∗ Worcester Polytechnic Institute
† Department of Physics
§ Department of Data Science

This study is supported by funding from the United States Department of Agriculture (Grant Number: USDA NR223A750013G032).

and adaptively selected to enable high-performance estimation of soil subsurface features. Thus, accurate soil subsurface characterization requires the development of a radar capable of changing its waveform and signal processing methods. The waveform spectrum, particularly its bandwidth, is crucial for radar range resolution. A higher bandwidth leads to finer resolution, but high-bandwidth radar hardware is very expensive. As an alternative, multiple narrowband signals are typically transmitted over multiple carrier frequencies to achieve high-resolution solutions, which FMCW (frequency-modulated continuous wave), SFCW, and OFDM (orthogonal frequency division multiplexing) waveforms are a few instances. [8][9][10][11][12].

This paper introduces the first GPR developed by the SoilX lab at Worcester Polytechnic Institute (WPI)[13]. The GPR specifically designed to facilitate waveform and frequency control facilitated by various waveforms and preprocessing operations through coding within the radar computer. The proposed Radar is developed using a low-cost spectrum analyzer capable of operating within the range of 0.2 - 1.5 GHz, which is essential for our experiment. To collect labeled data for soil moisture content extraction, we have conducted a field measurement campaign, and the labels were created via a moisture probe. We analyzed the collected GPR data to extract features that are closely related to soil moisture content. Here, we examined the mean of received power of the reflected transmitted signals, which is directly linked to soil moisture content. Different machine learning techniques such as Random Forest, Linear Regression, Lasso Regression, Decision Tree, and XGBoost were applied to extract moisture features. The results confirm that there is a relationship between the soil water content (SWC) and the amount of received power.

This paper is organized as follows. Section 2 introduces the Radar system design, Section 3 explains the experiment setup and measurement method, Section 4 analyzes data.

II. Radar System Design

GPR characterizes soil subsurface by analyzing backscattered signals that are formed by an interaction of the soil channel and the transmitted waveform. Soil channel is characterized by the soil electric features such as its relative electric permittivity, ϵ_r, which is determined by the soil texture, composition, and moisture (TCM). Thus, the received GPR signal includes the texture and moisture signatures of the soil subsurface [14]. Adoption of a proper frequency range is critical to extracting these signatures. For example, Fig. 1 shows frequency ranges (200 MHz to 1.5 GHz, L-band) within which the signal is considerably attenuated with soil moisture content. In addition, as shown in the figure there is a change in the slope of the attenuation at a certain frequency range which changes with moisture content. Thus, there are two pieces of information: (1) certain frequency ranges are critical to the extraction of moisture content, and (2) within that frequency range the attenuation features at certain frequencies are critical to moisture estimation. Our radar has been designed to operate within this frequency range to facilitate the creation of signatures that enable high-performance soil subsurface characterization.

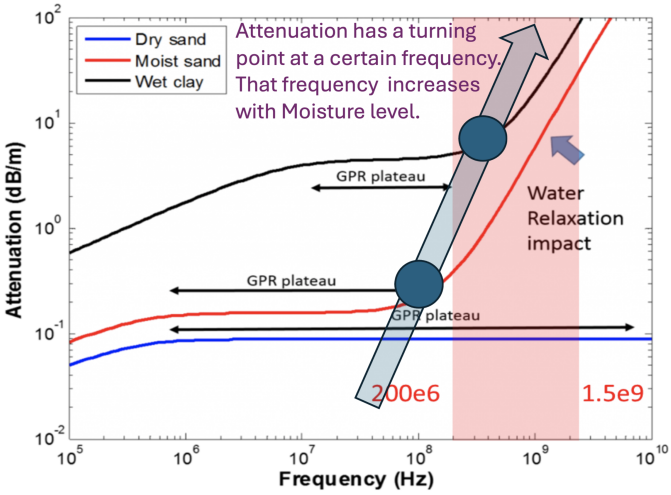

Fig. 1. Effective range of frequency to study soil water content from 200MHz to 1.5GHz. The graph shows how attenuation per depth (dB/m) changes for different amounts of moisture for a range of frequencies.

A. Radar Hardware Configuration

The designed and manufactured radar system consists of five main components: a transmitter (Signal Hound VSG25A), a receiver (Signal Hound SA44B), RF analog components such as power amplifiers, low-noise amplifiers, and low-pass filters, two log-periodic antennas for transmission and reception of EM signals, and a mini PC to operates the transceiver components and store received data. The transmitter can operate in the frequency range of 100MHz to 2.5GHz with a maximum output power of 10dBm (10mW), capable of transmitting different waveforms for adaptive design. The receiver works over a similar frequency range with a dynamic range from -151dBm to 10dBm in combination with the LNA, capturing reflected signals affected by the soil's electric permittivity. The lightweight, directional log-periodic antennas can work from 100MHz to 4GHz, making them suitable for airborne applications. A power amplifier with a gain of 10dB boosts the amplitude of the transmitted signal, resulting in an output power of 20dBm (100mW), enhancing the signal strength without adding excessive weight. Finally, a mini PC controls the transceiver components and manages data acquisition and storage, supporting real-time analysis and decision-making capabilities. This integrated radar system balances performance with practical considerations for airborne deployment, providing a reliable platform for analyzing soil features through the GPR technique.

B. Waveform Design

In this study, we use Pulse modulated SFCW to detect soil features. The transmitted pulse for a specific carrier frequency f_k is defined by:

$$s_k(t) = A \cdot g(t) \cdot \cos(2\pi f_k t), \quad k = 0, 1, 2, \ldots, 324. \quad (1)$$

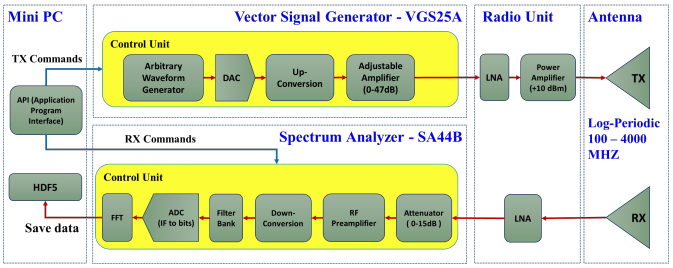

Fig. 2. Schematic of the radar configuration and the interconnections between components.

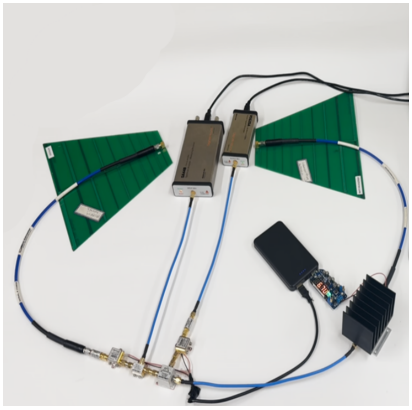

Fig. 3. Real photo of Manufactured Radar with the transmitter (VSG25A), the receiver (SA44B), log-periodic antenna, Power Amplifier, Low Noise Amplifiers and Low pass filters.

The constant amplitude A is 10 dBm. The baseband envelope $g(t) = rect\left(\frac{t-T_p}{\tau}\right)$ uses a pulse period T_p of 10 ms, pulse width τ of 300 µs. The carrier frequency $f_k = f_0 + k\Delta f$ starts at $f_0 = 200$ MHz and increases in $\Delta f = 4$ MHz steps. This SFCW signal spans 200-1500 MHz over 325 steps. Fig. 4 shows (a) the frequency increment over time and (b) the time-domain representation of the transmitted signal.

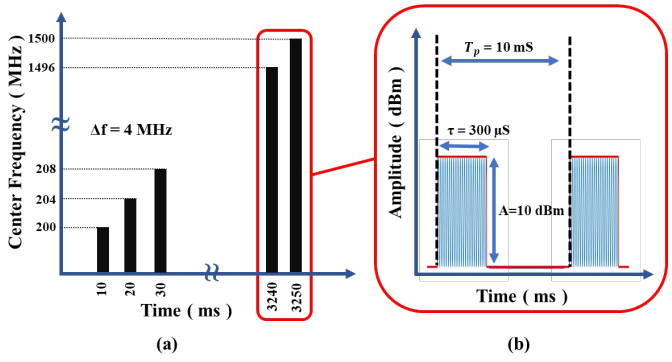

Fig. 4. Representation of Carrier frequency vs Time (a) and Amplitude vs Time (b) for Pulse modulated SFCW signal.

C. Signal Reception and Analysis

The radar receiver is equipped with an RF spectrum analyzer that can operate at different carrier frequencies ranging from 200MHz to 1500MHz. The received signal $\mathbf{r}_k$ for each frequency component, f_k, can be represented by:

$$\mathbf{r}_k(t) = \mathbf{s}_k(t) * \mathbf{h}_k(t) \quad , \quad k = 0, 1, 2, \ldots, 324. \tag{2}$$

Here, $\mathbf{s}_k(t)$ is the transmitted signal for the carrier frequency f_k and $\mathbf{h}_k(t)$ is the associated channel response. At the receiver, the received signal undergoes attenuation or amplification processes to ensure that it falls within the spectrum analyzer's dynamic range. Then, the signal is down-converted and passed through a filter bank to remove high-frequency noise. After that, the baseband received signal at each carrier frequency component is sampled using an analog-to-digital converter. Finally, a Fast Fourier Transform is performed by the spectrum analyzer to create 50,000 samples in the frequency domain. Accordingly, the received power spectrum of each carrier frequency component, f_k where $k = 0, 1, \ldots, 324$ corresponds to:

$$\mathbf{P}(f_k) = \{\gamma_m(f_k), m = -J+1, \ldots, J\}, \tag{3}$$

where $J = 25,000$, and γ_m, is the power in milli-watts for each of the 50,000 frequency samples.

We set up the receiver to receive all the 325 carrier frequencies transmitted step by step so that at the end of the i^{th} round of measurement, there are 325 received signal spectrums associated with 325 transmitted carrier frequencies. This process is performed automatically by the spectrum analyzer (SA44B) for each measurement. For a particular measurement i, we show a plot of $\mathbf{P}_i(f_k)$ at particular carrier frequency f_k in Fig.5 with frequency Hz in the x-axis and power in milliwatts (mW) for the y-axis. In the Plot, we can observe both the main lobe and accompanying side lobes of $\mathbf{P}_i(f_k)$. We have noticed for a particular measurement i, this plot varies over all 325 carrier frequency components. As the subsurface conditions change over multiple days with the flow of water, we have noticed for a particular carrier frequency f_k, the plots of $\mathbf{P}_i(f_k)$ exhibit variations as well. With this very raw version of the received GPR signal from our radar, we will perform feature engineering over each carrier frequency's individual $\mathbf{P}_i(f_k)$ and examine their usefulness in characterizing subsurface conditions.

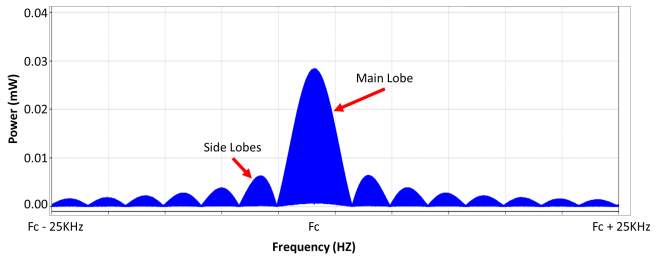

Fig. 5. A plot of a received power spectrum, $\mathbf{P}_i(f_c)$, from measurement i, for certain carrier frequency, f_c, over 50KHz frequency span. The y-axis shows the power in mW per frequency sample. Annotated are the main and side lobes.

III. Measurement Campaign

To evaluate our radar configuration and train machine learning models to estimate SWC, we conducted 24 rounds of measurement. Our measurement setup simulated a drone in flight over farmland with the radar consistently positioned at a height, H, of 1 meter above the ground, as shown in Fig.6. The moisture level of the target area was measured using 6 sleeves implanted in the ground by inserting the PR2 SDI-12 moisture probe [15]. The inserted probe measured the soil moisture in millivolts (mV), which we can convert to moisture percentage (%M) by the manufacture look-up table. The probe has the ability to measure mV and %M at 6 depths 10, 20, 30, 40, 60, and 100 cm when inserted into a sleeve.

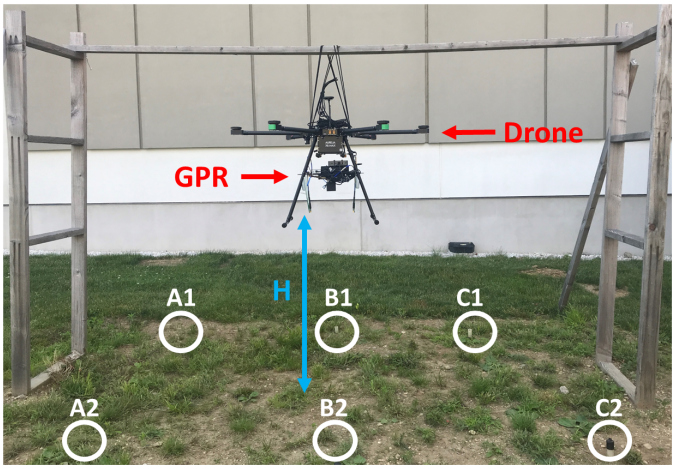

Fig. 6. Measurement Setup: measurements were taken via a suspended GPR-equipped drone. The TX and RX antennas of the GPR were positioned H = 1 meter above the ground surface. Six ground planted sleeves A1, A2, B1, B2, C1, and C2 used for assessment by the moisture probe.

From the 24 rounds of measurements, each GPR received signal $\mathbf{x}_i$, $i = 1, \ldots, 24$, can be represented as a vector of size 325, where each entry corresponded to the received impulse response at a particular carrier frequency:

$$\mathbf{x}_i = \{\mathbf{P}_i(f_k), k = 0, 1, \ldots, 324\}, \tag{4}$$

where $\{f_k, k = 0, \ldots, 324\}$ is the set of transmitted carrier frequencies and $\mathbf{P}_i(f_k)$ is set of size 50,000 of the received power spectrum for f_k. For each measurement i, we averaged mV readings across 6 locations (A1, A2, B1, B2, C1, C2; Fig. 6) at 6 depths to obtain:

$$\mathbf{y}_i = \{\bar{y}_d, d = 10, 20, 30, 40, 60, 100\}, \tag{5}$$

where $\bar{y}_d$ was the averaged probe measurement at depth d cm. This provided a mV reading representative of the soil subsurface area under the GPR at each depth. For later data analysis, we consider our dataset $D = \{(\mathbf{x}_i, \mathbf{y}_i)\}_{i=1}^{n=24}$ over all 24 measurements.

IV. Data Analysis Method

In this section, we appied machine learning (ML) models to explore whether any patterns can be revealed in the data from our radar, potentially providing information about subsurface properties. Towards this, we preprocessed our raw received GPR signals by feature engineering across each individual carrier frequency power spectrum and over our entire dataset. We then used our engineered features as input to a few ML models. If the models were successful in SWC prediction, it would support both the utility of our engineered features and the functionality of our new radar system in capturing soil subsurface characteristics.

A. Preprocessing Methods

As discussed in Section II-C, our radar was able to return a very raw form of each received carried frequency impulse response $\mathbf{P}_i(f_k)$ for a particular measurement i. From our 24 rounds of measurements, each GPR received signal $\mathbf{x}_i$, $i = 1, ..., 24$, can be represented as a vector of size 325, where each entry corresponds to the received impulse response's power spectrum at a particular carrier frequency:

$$\mathbf{x}_i = \left[\mathbf{P}_i(f_0), \quad \mathbf{P}_i(f_1), \quad \cdots, \quad \mathbf{P}_i(f_{324})\right]. \tag{6}$$

To distill each power spectrum into features to capture soil characteristics, we truncated each $\mathbf{P}_i(f_k)$ to only over a frequency range of 50 kHz frequencies around the center carrier frequency and calculated the mean power:

$$\bar{P}_i(f_k) = \frac{1}{2J} \sum_{j=-J+1}^{J} \gamma_j(f_k), \tag{7}$$

for $J = 25,000$ and $\gamma_j \in \mathbf{P}_i(f_k)$. This truncation accomplishes dimensionality reduction of each $\mathbf{P}_i(f_x)$ to a single scalar for later ML models to use all carrier frequency steps of the received signal. We expect when the subsurface soil conditions are constant, different frequencies will reflect back a different mean power. When the subsurface soil conditions were not constant over multiple measurements at different points in time, we expect variations in each particular carrier frequency's power spectrum's mean power.

For our dataset of 24 GPR received signals, $\mathbf{X} = [\mathbf{x}_1, \mathbf{x}_2, \cdots, \mathbf{x}_{24}]^T$, we normalized each column to have a mean of 0 and expressed the values in terms of standard deviation units from the mean. To achieve this, we applied Z-score normalization to each entry, $\bar{P}_i(f_k)$, of $\mathbf{X}$ as follows:

$$Z_i(f_k) = \frac{\bar{P}_i(f_k) - \mu_k}{\sigma_k}, \tag{8}$$

where μ_k, σ_k is the mean and standard deviation the values in column k or over the $\bar{P}_i(f_k))$ for $i = 1, \ldots, 24$ [16]. This normalization ensured that each column or feature in $\mathbf{X}$ was on the same scale for later ML training.

B. Model Training Methods

We evaluated several machine learning models: Linear Regression (LR), Lasso, Decision Tree (DT), Random Forest (RF), XGBoosted Random Forest (XGB), and a Dummy Regressor (DUM) [16]. The models, except for DUM, used Z-score normalized mean power per carrier frequency power

TABLE I
AVERAGE ML MODEL PERFORMANCE PREDICTING MV (0 TO 1000) OVER ALL DEPTHS WITH ± STANDARD ERROR. THE MODEL WHICH OBTAINED THE LOWEST OVERALL RMSE IS SHOWN IN GREEN.

Model/Metric	RMSE (mV)
Linear Regression	116 ± 6
Lasso	**99 ± 6**
RF	114 ± 5
XGB	146 ± 8
DT	102 ± 8
DUM	205 ± 8

spectrum as input data. DUM served as a baseline model that does not use any GPR data. It predicted SWC by averaging probe measurements from the training set to estimate probe measurements in the test set. The other ML models used GPR data from the new radar. If these models outperformed DUM, it would support our radar system's responsiveness to changes in subsurface media, like SWC. However, if DUM provided more accurate SWC predictions without GPR data, this may indicate one or more of the following issues: (1) the GPR system may not be sufficiently responsive to changes in subsurface conditions; (2) the selected ML models may not be suited to make reliable predictions from the input GPR signals; (3) the engineered feature extracted, $\bar{P}_i(f_k)$, may not be useful for predicting SWC.

We used the root mean squared error (RMSE) as a metric to evaluate the model performance [16]. The RMSE was defined as:

$$\text{RMSE} = \sqrt{\frac{1}{n|\mathbf{y}|}\sum_{i=1}^{n}\|\mathbf{y}_i - \hat{\mathbf{y}}_i\|^2}, \tag{9}$$

where n is the number of measurements, $|\mathbf{y}| = 6$ is the length of the vector of probe measurements when predicting all depths, and $|\mathbf{y}| = 1$ when presenting results for a specific depths.

To address the challenges posed by our limited dataset of 24 samples, we implemented a Leave-One-Out Cross Validation (LOOCV) combined with an inner 5-Fold Cross Validation [16]. For each of the 24 data points, 23 were used for training and 1 for testing. Within each LOOCV iteration, we performed an inner 5-fold cross-validation on the 23 training GPR received signal samples to tune the model hyperparameters.

The optimal parameters are selected by minimizing the RMSE between the ground truth values, $\mathbf{y}_i$, and the predicted values, $\hat{\mathbf{y}}_i$, across all training data points. The RMSE is calculated based on (9) with $|\mathbf{y}| = 6$ and $n = 19$ for the number of training data points in each inner fold. This parameter selection process ensured generalization as best as possible across different probe depths and training subsets to unseen test points. The selected model with the best set of parameters from this inner loop was then applied to all 23 samples and used to predict the held-out test point. This process was repeated for all 24 samples. We reported the overall average RMSE over all depths with standard error average over all the held-out test points in Table I and per depth in Table II.

C. Results

Table I presented the average RMSE (see (9) with $|\mathbf{y}| = 6$) results. We observed that Lasso had the lowest RMSE over all depths. The Tree-based models showed similar performance, while XGB stood out with the highest RMSE at 146 ± 8 mV, which may have overfitted on the small dataset.

Table II presented soil moisture results per depth (see (9) with $|\mathbf{y}| = 1$). It was observed that for depths 10, 20, and 30 cm, Lasso achieved the lowest RMSE between the ground truth %M and the predicted. At these initial 3 depths, all ML models had a lower RMSE than the DUM model by up to 54 percent, which supports our GPR system's functionality. This also showed that adopting $\bar{P}_i(f_k)$ as a feature may enabled an adequate soil moisture prediction at shallow depths by our selected ML models. For depths 40 cm and below, we saw few ML models outperform DUM by a very small margin. This pointed to a limitation of the ability for $\bar{P}_i(f_k)$ to capture variations in soil characteristics at lower depths. This suggested that predicting subsurface SWC at deeper soil layers may require a more focused feature engineering approaches to characterize deeper layers of the subsurface soil.

V. CONCLUSION

The paper introduces a new SFCW GPR that facilitates the acquisition of a data set across multiple frequency bands, which makes it uniquely suitable for ML-based soil subsurface moisture estimation. The team conducted a measurement campaign over the summer of 2024 to collect the data. Moisture probe readings across multiple depths serve as ground truth labels per GPR measurement. The power spectrum of each carrier frequency provided by our GPR contains a variety of features which can be extracted and leveraged for moisture-depth estimation. The paper considers the average power per carrier frequency as the feature and assesses the performance of a set of ML models for subsurface soil moisture estimation. The results confirm the utility of this feature as input to ML models at near surface depths and supports our new GPR system's functionality. This study is considered the first attempt to assess moisture information with our custom radar. Our future work will investigate and compare other feature engineering approaches on the received GPR signal. The measurement campaign was conducted at WPI grounds. Our future measurements will be organized at local farms and will include comprehensive measurement campaigns that collect a large amount of data at different altitudes.

ACKNOWLEDGMENT

We would like to thank Ethan Reed and Nicholas Latsis, undergrad students at Worcester Polytechnic Institute, for their support of the project.

TABLE II

PERFORMANCE ASSESSMENT OF MOISTURE ESTIMATION AT DIFFERENT DEPTHS IN TERMS OF %M RMSE WITH ± STANDARD ERROR. %M (0 TO 100) CALCULATED FROM MV BY PROBE MANUFACTURER'S LOOK-UP TABLE. IN GREEN ARE THE MODELS WITH THE LOWEST OBSERVED RMSE FOR EACH SUBSURFACE DEPTH (CM).

Model / Depth	10 cm	20 cm	30 cm	40 cm	60 cm	100 cm
Lasso	**5.4 ± 0.2**	**5.2 ± 0.2**	**5.6 ± 0.2**	19.0 ± 0.7	20.1 ± 0.8	17.9 ± 0.7
RF	6.7 ± 0.3	5.6 ± 0.1	6.1 ± 0.1	18.6 ± 0.4	17.6 ± 0.6	18.2 ± 0.7
LR	5.8 ± 0.1	6.2 ± 0.1	5.9 ± 0.1	19.5 ± 0.2	21.7 ± 0.2	**17.5 ± 0.2**
XGB	6.9 ± 0.1	6.5 ± 0.1	7.0 ± 0.1	29.8 ± 0.3	29.4 ± 0.3	30.8 ± 0.3
DT	7.6 ± 0.1	6.0 ± 0.1	7.0 ± 0.1	18.6 ± 0.2	**16.0 ± 0.2**	18.3 ± 0.2
DUM	11.9 ± 0.1	10.1 ± 0.1	10.5 ± 0.1	**17.9 ± 0.2**	17.9 ± 0.2	17.8 ± 0.2

REFERENCES

[1] D. N. Moriasi, J. G. Arnold, M. W. Van Liew, R. L. Bingner, R. D. Harmel, and T. L. Veith, "Model Evaluation Guidelines for Systematic Quantification of Accuracy in Watershed Simulations," *Transactions of the ASABE*, vol. 50, no. 3, pp. 885–900, 2007.

[2] V. Filardi, A. Cheung, R. Khan, O. Mangoubi, M. Moradikia, S. R. Zekavat, B. Wilson, R. Askari, and D. Petkie, "Data-Driven Soil Water Content Estimation at Multiple Depths Using SFCW GPR," in *2023 IEEE International Opportunity Research Scholars Symposium (ORSS)*, (Atlanta, GA, USA), pp. 86–90, IEEE, Apr. 2023.

[3] H. Namdari, M. Moradikia, D. T. Petkie, R. Askari, and S. Zekavat, "Comprehensive GPR Signal Analysis via Descriptive Statistics and Machine Learning," in *2023 IEEE International Conference on Wireless for Space and Extreme Environments (WiSEE)*, pp. 127–132, Sept. 2023. ISSN: 2380-7636.

[4] H. Namdari, M. Moradikia, R. Askari, O. Mangoubi, and D. Petkie, "Advancing Precision Agriculture: Machine Learning-Enhanced GPR Analysis for Root-Zone Soil Moisture Assessment in Mega Farms," Apr. 2024.

[5] S. Senanayake, B. Pradhan, A. Huete, and J. Brennan, "Assessing Soil Erosion Hazards Using Land-Use Change and Landslide Frequency Ratio Method: A Case Study of Sabaragamuwa Province, Sri Lanka," *Remote Sensing*, vol. 12, p. 1483, May 2020.

[6] B. R. Scanlon, B. L. Ruddell, P. M. Reed, R. I. Hook, C. Zheng, V. C. Tidwell, and S. Siebert, "The food-energy-water nexus: Transforming science for society," *Water Resources Research*, vol. 53, no. 5, pp. 3550–3556, 2017.

[7] M. Rodell, J. S. Famiglietti, D. N. Wiese, J. T. Reager, H. K. Beaudoing, F. W. Landerer, and M.-H. Lo, "Emerging trends in global freshwater availability," *Nature*, vol. 557, pp. 651–659, May 2018. Publisher: Nature Publishing Group.

[8] J. Platt, Y.-K. Hong, H. Won, O. Olaniyan, M. Choi, and J. Lee, "Simulation of FMCW and M-Sequence Ground Penetrating Radar Systems," in *2022 IEEE Radio and Wireless Symposium (RWS)*, pp. 142–145, Jan. 2022. ISSN: 2164-2974.

[9] S. Zheng, X. Pan, A. Zhang, Y. Jiang, and W. Wang, "Estimation of Echo Amplitude and Time Delay for OFDM-Based Ground-Penetrating Radar," *IEEE Geoscience and Remote Sensing Letters*, vol. 12, pp. 2384–2388, Dec. 2015. Conference Name: IEEE Geoscience and Remote Sensing Letters.

[10] M. Metwally, N. L'Esperance, and T. Xia, "Ground penetrating radar utilizing compressive sampling and OFDM techniques," in *2015 IEEE International Symposium on Circuits and Systems (ISCAS)*, pp. 2117–2120, May 2015. ISSN: 2158-1525.

[11] G. Tronca, I. Tsalicoalou, S. Lehner, and G. Catanzariti, "Comparison of pulsed and stepped frequency continuous wave (SFCW) GPR systems," in *2018 17th International Conference on Ground Penetrating Radar (GPR)*, pp. 1–4, June 2018. ISSN: 2474-3844.

[12] P. Smogavec, B. Pongrac, and D. Gleich, "Evaluation of Compact and Modular SFCW GPR Systems for Detecting Buried Objects," in *2023 30th International Conference on Systems, Signals and Image Processing (IWSSIP)*, pp. 1–5, June 2023. ISSN: 2157-8702.

[13] "Soilx Website: https://soilx.wpi.edu/."

[14] H. M. Jol, *Ground penetrating radar: theory and applications*. Amsterdam, Netherlands Oxford, UK: Elsevier Science, 1st ed ed., 2009.

[15] "PR2 Profile Probe - SDI-12: https://delta-t.co.uk/pr2-profile-probe-sdi-12-version/."

[16] G. James, D. Witten, T. Hastie, and R. Tibshirani, *An Introduction to Statistical Learning: with Applications in R*. New York Heidelberg Dordrecht London: Springer, 1st ed. 2013, corr. 7th printing 2017 edition ed., June 2013.